[redacted]

213

Copy
RM L55H22a

NACA RM L55H22a

7640

TECH LIBRARY KAFB, NM
0144112

Reg # 10021

NACA

RESEARCH MEMORANDUM

FLIGHT DETERMINATION OF DRAG AND PRESSURE RECOVERY OF TWO SCOOP INLETS LOCATED AT MAXIMUM-BODY-DIAMETER STATION AT MACH NUMBERS FROM 0.8 TO 1.8

By Leonard W. Putland

Langley Aeronautical Laboratory
Langley Field, Va.

HADC
TECHNICAL LIBRARY
AFL 2811

[redacted]

This material contains information affecting the National Defense of the United States within the meaning of the [redacted]

NATIONAL ADVISORY COMMITTEE
FOR AERONAUTICS

WASHINGTON
January 10, 1956

[redacted]

Classification cancelled (or changed to UNCLASSIFIED)

By Authority of NASA Tech Pub Announcement #4
(OFFICER AUTHORIZED TO CHANGE)

By ..... 14 Nov 58
NAME AND

[signature]
GRADE OF OFFICER MAKING CHANGE)

[illegible] Oct 61
DATE

TECH LIBRARY KAFB, NM
0144112

NATIONAL ADVISORY COMMITTEE FOR AERONAUTICS

RESEARCH MEMORANDUM

FLIGHT DETERMINATION OF DRAG AND PRESSURE RECOVERY OF TWO SCOOP INLETS LOCATED AT MAXIMUM-BODY-DIAMETER STATION AT MACH NUMBERS FROM 0.8 TO 1.8

By Leonard W. Putland

SUMMARY

Two models each utilizing a scoop inlet located at the maximum-body-diameter station operating at mass-flow ratios from 0.76 to 0.96 have been flight-tested at an angle of attack of approximately 0° over a Mach number range from 0.8 to 1.8, and a Reynolds number range from 2×10^6 to 7×10^6 based on body maximum diameter. One of the scoop inlets had a circular cross section with a boundary-layer diverter. The other scoop inlet had a semicircular cross section wrapped partly around the body with a boundary-layer splitter plate ahead of the inlet.

There was no significant difference between the total-pressure recovery at the top and bottom of the duct of the two scoop-inlet models except for the semicircular scoop-inlet model below Mach number 1.3. For this inlet the total-pressure recovery at the top of the duct was greater than that for the bottom of the duct. The mean total-pressure recovery for the semicircular scoop-inlet models was less than the circular scoop-inlet model throughout the Mach number range.

The external drag coefficients above Mach number 1.3 were identical for the two scoop-inlet models. Between Mach numbers 1.0 and 1.3, the external drag coefficient of the circular scoop-inlet model was higher than that of the semicircular scoop-inlet model. The external drag coefficients for the scoop-inlet models were higher than the drag coefficients for the basic nonducted model throughout the Mach number range tested.

[redacted]

INTRODUCTION

The total-pressure recovery of an air inlet and the effect of its installation on the drag of the configuration are two important considerations involved in the selection of a particular inlet configuration. A scoop-inlet configuration has become important since the nose of airplanes and missiles has become more in demand for electronic and armament purposes. This investigation was conducted to determine some of the effects of a circular and a wraparound semicircular scoop inlet located at the maximum-body-diameter station. The maximum diameter was chosen to minimize the ducting to a theoretical engine in the rear of the configuration.

The scoop-inlet configurations have been flight-tested using rocket-propelled models in free flight at an angle of attack of approximately 0° by the Pilotless Aircraft Research Division of the Langley Aeronautical Laboratory. The results of these tests are presented herein in the form of external drag coefficients and total-pressure recoveries over a range of Mach numbers from 0.8 to 1.8. The drag of the basic parabolic body from reference 1 is also included for comparison.

SYMBOLS

A area

A_i inlet capture area (for circular scoop inlet, 0.0506 sq ft; for semicircular scoop inlet, 0.0498 sq ft)

C_D drag coefficient, $\dfrac{D}{\frac{1}{2}\rho_o V_o^2 A_F}$

D drag

l total body length

M Mach number

p static pressure

p_t stagnation pressure

p_d' total-head pressure measured by a total-head tube at duct measuring station

$p_{t,d}$ mean duct total pressure

q dynamic pressure, $\frac{1}{2}\rho V^2$

R Reynolds number, based on body maximum diameter

r radius

V velocity

w/w_o ratio of mass flow of air through duct to mass flow of air through a free-stream tube of area equal to inlet capture area

x longitudinal distance

γ ratio of specific heats, 1.40 for air

ρ air density

Subscripts:

d duct measuring station

e exit

F frontal

o free stream

ext external

int internal

MODELS

The general arrangements of the two inlet models are shown in figure 1 and the basic and inlet body coordinates are listed in table I. The body of each of the models was constructed from mahogany and had fineness ratios of 3.6, 2.0, and 5.3 for the parabolic nose, cylindrical center section, and parabolic afterbody, respectively. The basic body from reference 1 consisted of a parabolic nose with a fineness ratio of 3.6 and a parabolic afterbody with a fineness ratio of 5.8. The models were stabilized by four 60° delta fins as shown in figure 1.

Except for the inlets, internal ducting, and the inlet external fairing to station 43.30, the two inlet models were identical. Both the

scoop inlets were located at the maximum-body-diameter station and were designed to have an inlet capture area of about 19 percent of the body frontal area. The inlet and ducting details are shown in figure 2.

One of the inlet models had a scoop inlet with a circular cross section swept 6° and utilized a boundary-layer diverter 1/4 inch high having a total divergence angle of 45°. The capture area of 0.0506 square foot was defined by the inlet lips. There was an internal contraction of 0.847. The other inlet model had a scoop inlet with a semicircular cross section wrapped around the body. This inlet had a boundary-layer splitter plate $\frac{1}{4}$ inch high and extending $1\frac{1}{4}$ inches forward of the inlet. The capture area of this inlet was defined as the projected frontal area of the leading edge of the inlet lips and boundary-layer splitter plate. There was a 6° angle on the splitter plate which produced some external compression. This inlet had no internal contraction. The ratios of inlet area to duct-measuring-station area for the circular and semicircular scoop-inlet models were 0.446 and 0.438, respectively. The exit area was about 15 percent less than the inlet area for both the scoop-inlet models. This exit area was so selected that the inlet would operate at slightly less than maximum mass flow. At these mass flows the spillage drag would be near the minimum while the pressure recovery would be near the maximum.

Photographs of the models, showing the general arrangement and inlet closeup, are presented as figures 3(a) and (b). The photograph of the typical model-booster arrangement is presented as figure 3(c). Figure 4 presents the area distribution as a function of the longitudinal distance. The cross-sectional area distribution of the two scoop-inlet models and the basic body are presented in figure 4(a). In figure 4(b) the area distribution of the duct perpendicular to the duct center line is presented for both scoop-inlet models.

TEST AND INSTRUMENTATION

All models were propelled to maximum Mach number by a single-booster, 6-inch ABL Deacon rocket motor, equipped with four stabilizing fins. The models were launched at an elevation angle of 60° and followed a zero-lift trajectory at approximately 0° angle of attack. The variation of change of Reynolds number with Mach number is shown in figure 5. The tests were conducted at the Langley Pilotless Aircraft Research Station at Wallops Island, Va.

Total-drag data were obtained during the decelerating portion of the flight, after drag separation of the booster. Computations were based on the CW Doppler radar velocity measurements (corrected for flight-path curvature and winds aloft), the NACA modified SCR-584 radar trajectory

measurements, and radiosonde atmospheric measurements. Details of the method of computation are presented in reference 2.

A four-channel telemeter was used to make the measurements to determine the internal flow characteristics. The four pressures which were measured continuously during the flight were the lower and upper duct total pressures, the four manifolded duct static pressures, and the exit static pressure. The lower and upper duct total pressures were measured differentially to improve the comparable accuracy. The arrangements of the duct pressure tubes are shown in figure 2. The exit static pressure was measured at the end of the constant-area section of the convergent insert of the exit. This convergent insert was made cylindrical for 1.05 exit diameters ahead of the exit to aid in providing uniform static pressure at the exit. A fairly large contraction ratio of 3.2 to 1 from the station just rearward of the duct measuring station to the exit assured sonic rather than supersonic exit velocities at supersonic speeds and helped to provide uniform total pressure at the exit.

DATA REDUCTION

The mass-flow ratio was calculated from the measured value of the exit static pressure and an exit Mach number obtained by assuming $p_{t,e} = p_d$, that is, a total pressure loss of 1 "q", from the duct measuring station to the exit. This assumption of a 1 "q" total pressure loss was checked at supersonic speeds where the exit Mach number was sonic and was found to be well within the estimated accuracies. The mean duct total-pressure recovery was calculated from the duct static-pressure measurements and the average duct Mach number obtained from the continuity relationship between the duct measuring station and the exit.

The internal drag was obtained by applying the momentum equation between the free stream ahead of the model and the duct exit:

$$D_{int} = \gamma p_o M_o^2 A_1\left(\frac{W}{W_o}\right) - \gamma p_e M_e^2 A_e - \left(p_e - p_o\right)A_e$$

At subsonic speeds when the exit was no longer sonic, the internal drag was assumed constant at the value at $M_o = 1.0$, as done in reference 3.

The external drag is defined herein as the sum of the dragwise components of the aerodynamic pressure and viscous forces acting on the external surfaces of the model plus the scoop incremental drag, as defined in reference 4. Scoop incremental drag is the algebraic sum of

the pressure drag on the entering stream tube and the pressure and viscous drags on that portion of the body (if any) wetted by the entering flow. The external drag was obtained by subtracting the internal drag from the total drag determined from the Doppler radar.

From the consideration of the accuracies of the measurements, the method of data reduction, and the previous experience with ducted models, the data are estimated to be accurate within the following limits throughout the Mach number range:

$\Delta \frac{p_d'}{p_{t,o}}$ and $\Delta \frac{\overline{p_{t,d}}}{p_{t,o}}$ . . . . . ±0.01

$\Delta \frac{w}{w_o}$ . . . . . ±0.01

$\Delta C_{D_{ext}}$ . . . . . ±0.01

ΔM_o . . . . . ±0.01

RESULTS AND DISCUSSION

The total-pressure recovery, mass-flow ratio, and internal drag coefficient are presented in figure 6 as a function of Mach number for both scoop-inlet models. For the circular scoop-inlet models (fig. 6(a)), there was no significant difference between the recoveries measured by the upper and lower total-pressure tubes. The mean total-pressure recovery calculated from the duct static pressure was as high as or higher than the individual tube measurements throughout the Mach number range.

For the semicircular scoop-inlet model (fig. 6(b)), below Mach number 1.3, the recovery measured by the upper total-pressure tube was 7 percent greater than that measured by the lower total-pressure tube. At higher Mach numbers this trend was reversed, until at $M_o \approx 1.7$ the upper total-pressure tube measured a recovery about 3 percent less than the lower tube. This might be expected when the geometry of the inlet is considered. For $M > 1.4$, the shock system associated with the semicircular scoop is such that the air entering the upper portion of the inlet passed through a single strong shock, while the air entering the lower portion of the duct passed through an oblique shock before passing through the strong shock. However, the mean total-pressure recovery calculated from the duct static pressure agrees well with the average of the two individual tube measurements throughout the Mach number range.

Figure 7 presents the comparison as a function of Mach number between the mean total-pressure recoveries for both scoop-inlet models with the free-stream normal-shock recovery. The mean total-pressure recovery for the circular scoop-inlet model showed approximately a constant diffuser loss of about 4 percent from free-stream normal-shock recovery over the lower portion of the Mach number range. This indicates there is no significant boundary-layer problem with this type of inlet. At the higher Mach numbers, the losses are somewhat greater. This may be caused by the local superstream Mach number ahead of the inlet being increased because of the parabolic forebody.

The semicircular scoop-inlet model had a lower mean total-pressure recovery than the circular scoop-inlet model over the Mach number range. The loss in total-pressure recovery from free-stream normal shock was not constant. At Mach number near 1.0, the total-pressure recovery for the semicircular scoop-inlet model was about 3 percent below the circular scoop-inlet model. This shows a higher diffuser loss for the semicircular scoop inlet. As the Mach number is increased to near Mach number 1.4, the pressure recovery of the semicircular scoop-inlet model is 1 percent below that of the circular scoop-inlet model. The decrease of the difference in pressure recovery between the two scoop-inlet models was possibly due to the improvement of the inlet-shock pattern as the result of the 6° splitter plate used on the semicircular scoop inlet. At the higher Mach numbers, the difference in pressure recovery between the two inlet models increased to 5 percent.

Figure 8 presents the comparison as a function of Mach number between the external drag coefficient for the two scoop-inlet models with the drag coefficient for the basic nonducted model (fineness-ratio-3.6 nose) of reference 1. This drag coefficient of the basic body is presented as the total minus base drag coefficient (both from ref. 1) plus a skin-friction-drag correction determined from reference 5 for the fineness-ratio-2 cylindrical section of the inlet models.

The external drag coefficients above Mach number 1.3 were identical for the two scoop-inlet models. Below Mach number 1.3, the difference in the external drag increased with the circular scoop-inlet model having the higher drag. The same results were also found between the circular and semicircular scoop-inlet models of reference 6.

The external drag coefficient of the inlet models was about 34 percent greater than the basic-body drag coefficient above Mach number 1.3. The major portion of this drag difference is probably composed of the drag associated with the fairing of the scoop into the body. The scoop incremental drag also accounts for some of the drag difference. An improvement in drag would be expected by locating the inlet forward of the present maximum-diameter location. In references 7 and 8, the installation of a scoop inlet well forward on the body resulted in no significant difference

in drag as compared with the drag of the body alone. Moving the inlet forward will also improve the inlet mass-flow ratio and total-pressure recovery. At this inlet location, the local Mach number due to the parabolic forebody would be less.

The subsonic level of the circular scoop-inlet model was 47 percent greater than the basic body. This drag difference was greater than the increase in skin-friction drag associated with the larger wetted area. This increase over the skin-friction-drag difference is believed to be interference effects of the inlet and ducting installation. A similar effect for a circular scoop inlet is shown in reference 6.

CONCLUSIONS

Two models with a scoop inlet located at the maximum-body-diameter station and employing a boundary-layer bypass were tested over a range of mass-flow ratios from 0.76 to 0.96 and Mach numbers from 0.8 to 1.8 at zero angle of attack. One of the scoops had a circular cross section while the other had a semicircular cross section wrapped around the body. The results of these tests and comparison with previously published data indicate the following conclusions:

1. For the semicircular scoop-inlet model, the total-pressure recovery at the top of the duct was about 7 percent greater than that at the bottom of the duct below Mach number 1.3 whereas there was no significant difference between the recoveries for the circular scoop-inlet model.

2. The mean total-pressure recovery for the semicircular scoop-inlet model was less than the circular scoop-inlet model, throughout the Mach number range.

3. The external drag coefficients above Mach number 1.3 were identical for the two scoop-inlet models. Between Mach numbers 1.0 and 1.3, the external drag coefficient of the circular scoop-inlet model was higher than that of the semicircular scoop-inlet model.

4. The external drag coefficient of the scoop-inlet models was about 34 percent greater than the basic-body drag coefficient above Mach number 1.3.

5. The subsonic drag level of the circular scoop-inlet model was 47 percent greater than the basic body drag. This drag difference was greater than the increase in skin-friction drag associated with the larger wetted area.

Langley Aeronautical Laboratory,
National Advisory Committee for Aeronautics,
Langley Field, Va., August 10, 1955.

REFERENCES

1. Sears, R. I., Merlet, C. F., and Putland, L. W.: Flight Determination of Drag of Normal-Shock Nose Inlets With Various Cowling Profiles at Mach Numbers From 0.9 to 1.5. NACA RM L53I25a, 1953.

2. Wallskog, Harvey A., and Hart, Roger G.: Investigation of the Drag of Blunt-Nosed Bodies of Revolution in Free Flight at Mach Numbers From 0.6 to 2.3. NACA RM L53D14a, 1953.

3. Merlet, Charles F., and Putland, Leonard W.: Flight Determination of the Drag of Conical-Shock Nose Inlets With Various Cowling Shapes and Axial Position of the Center Body at Mach Numbers From 0.8 to 2.0. NACA RM L54G21a, 1954.

4. Klein, Harold: The Calculation of the Scoop Drag for a General Configuration in a Supersonic Stream. Rep. No. SM-13744, Douglas Aircraft Co., Inc., Apr. 12, 1950.

5. Van Driest, E. R.: Turbulent Boundary Layer in Compressible Fluids. Jour. Aero. Sci., vol. 18, no. 3, Mar. 1951, pp. 145-160, 216.

6. Judd, Joseph H.: A Free-Flight Investigation of the Drag Coefficients of Two Single-Engine Supersonic Interceptor Configurations From Mach Numbers 0.8 to 1.9 To Determine the Effect of Inlet and Engine Locations. NACA RM L55G05a, 1955.

7. Merlet, Charles F.: Pressure Recovery and Drag Characteristics of a Forward Located Circular Scoop Inlet As Determined From Flight Tests for Mach Numbers From 0.8 to 1.6. NACA RM L54B23, 1954.

8. Pierpont, P. Kenneth, and Braden, John A.: Investigation at Transonic Speeds of a Forward-Located Underslung Air Inlet on a Body of Revolution. NACA RM L52K17, 1953.

TABLE I.- BODY COORDINATES

[All dimensions in inches]

Basic body (ref. 1)

x	r
0	0
1.00	.27
2.00	.53
3.00	.78
4.00	1.02
5.00	1.25
7.00	1.67
10.00	2.23
15.00	2.93
20.00	3.35
25.20	3.50
30.80	3.45
35.47	3.34
41.07	3.14
46.67	2.84
49.47	2.65
56.00	2.15
60.90	1.68
65.68	1.16

Scoop-inlet body

x	r
0	0
1.00	.27
2.00	.53
3.00	.78
4.00	1.02
5.00	1.25
7.00	1.67
10.00	2.23
15.00	2.93
20.00	3.35
25.20	3.50
39.20	3.50
44.80	3.45
49.47	3.34
55.07	3.14
60.67	2.84
63.47	2.65
70.00	2.15
74.90	1.68
76.30	1.53

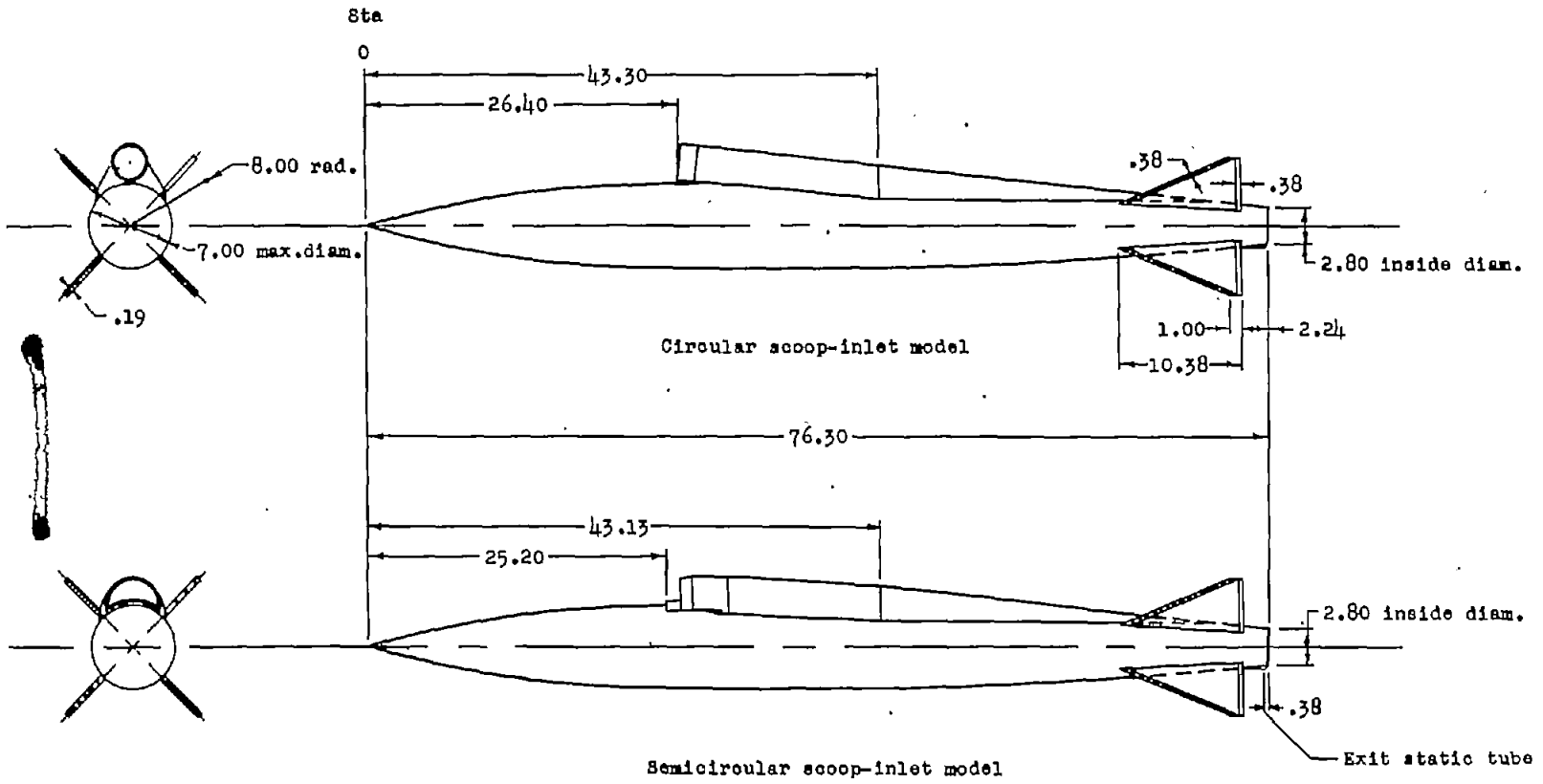

Figure 1.- General arrangement of models. (All dimensions are in inches.)

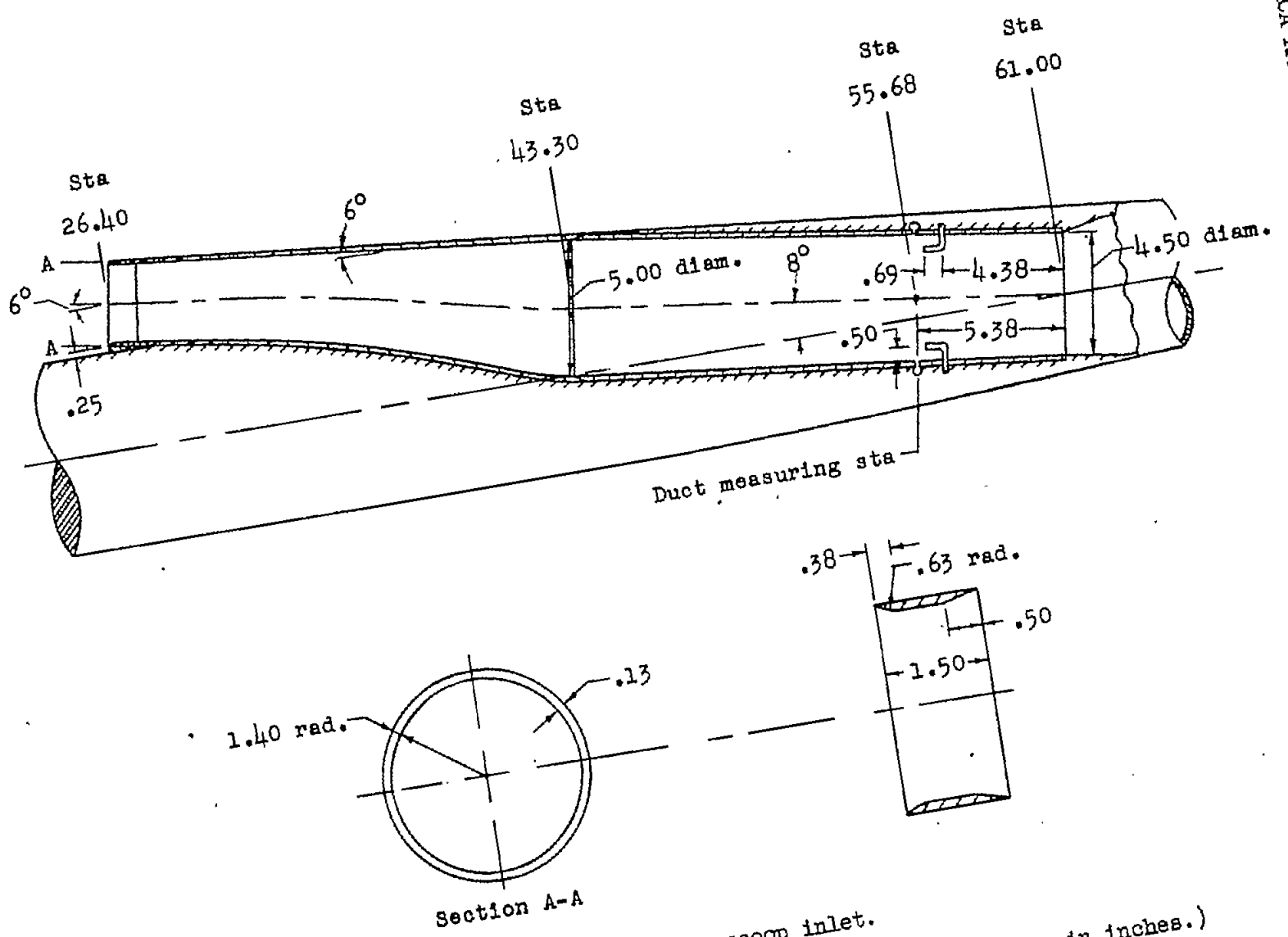

(a) Circular scoop inlet.

Figure 2.- Details of inlets and ducting. (All dimensions are in inches.)

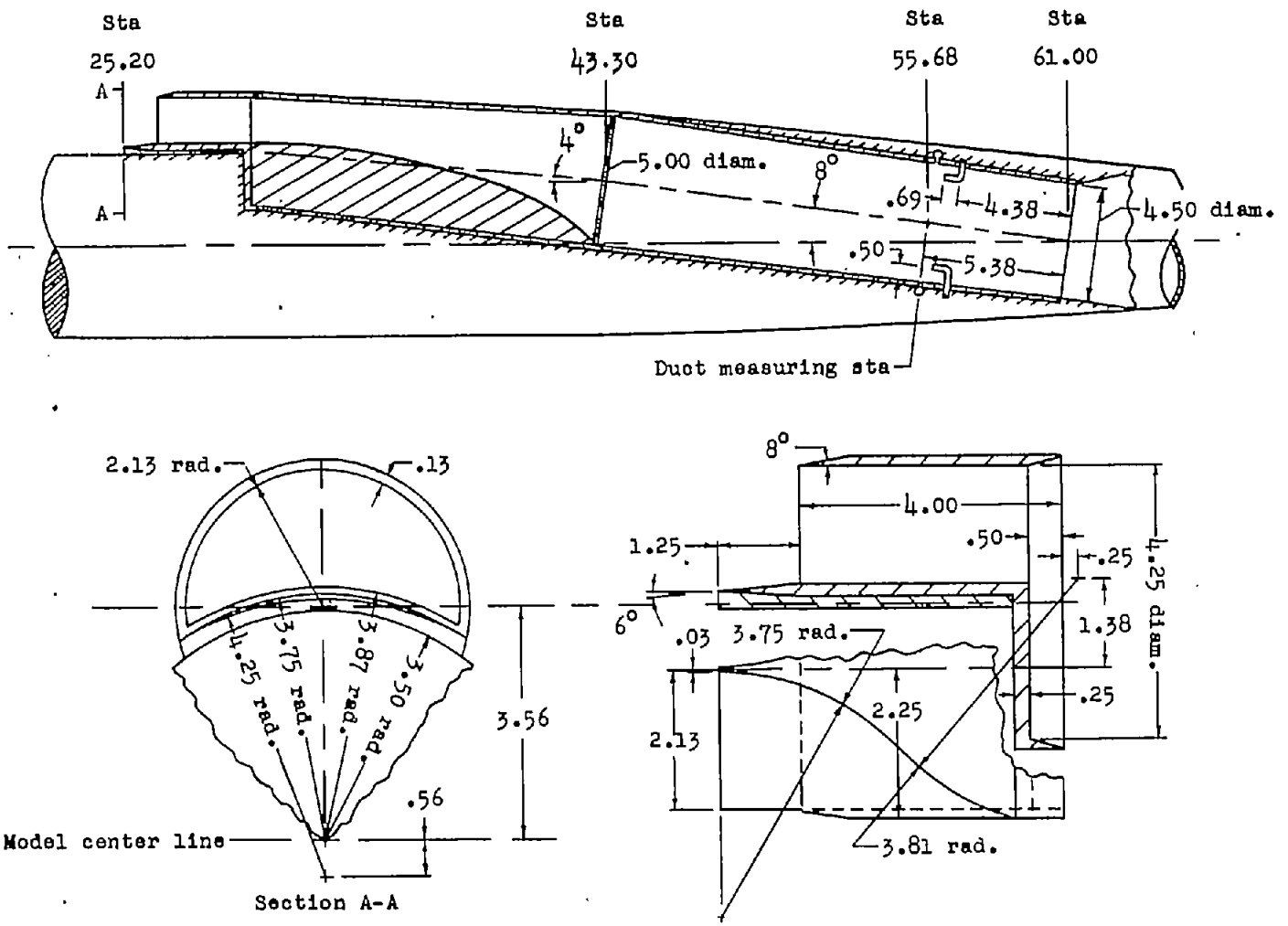

(b) Semicircular scoop inlet.

Figure 2.- Concluded.

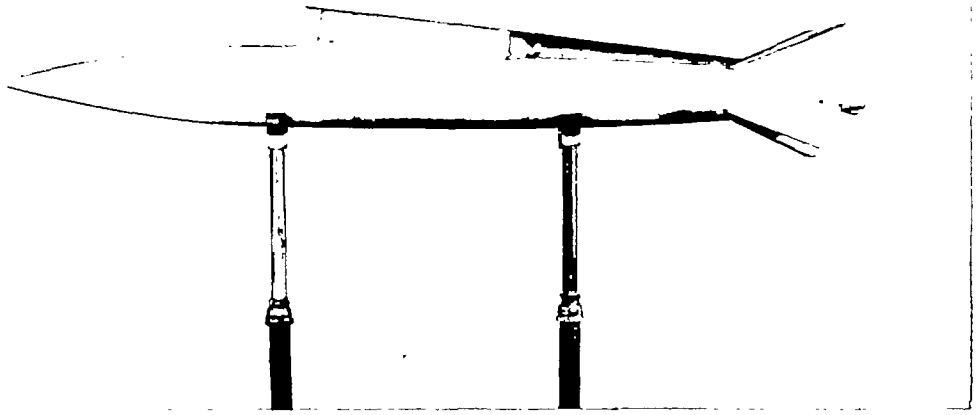

L-83046.1

Circular scoop inlet

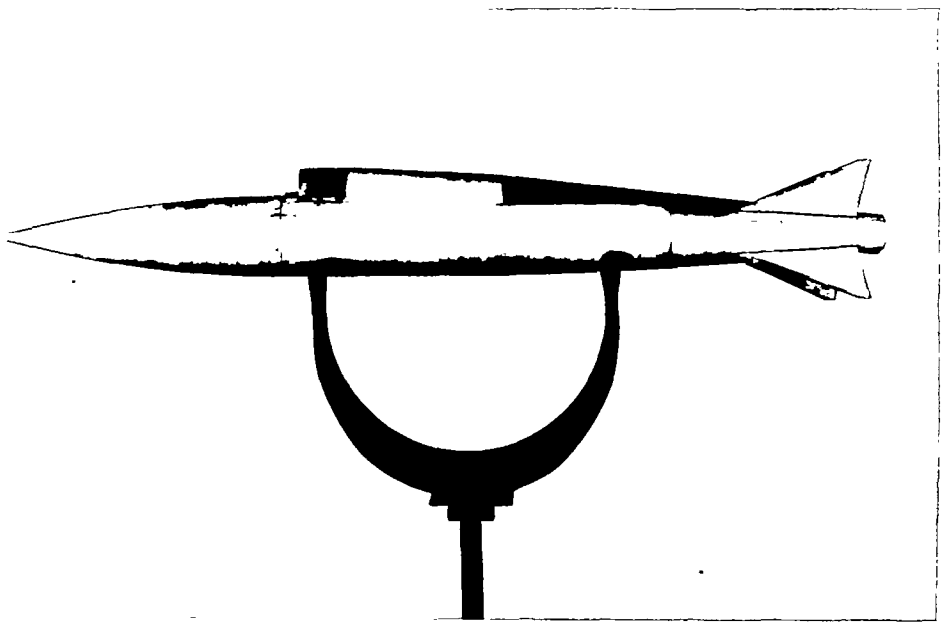

Semicircular scoop inlet

L-83499.1

(a) General views.

Figure 3.- Photographs of models.

[redacted]

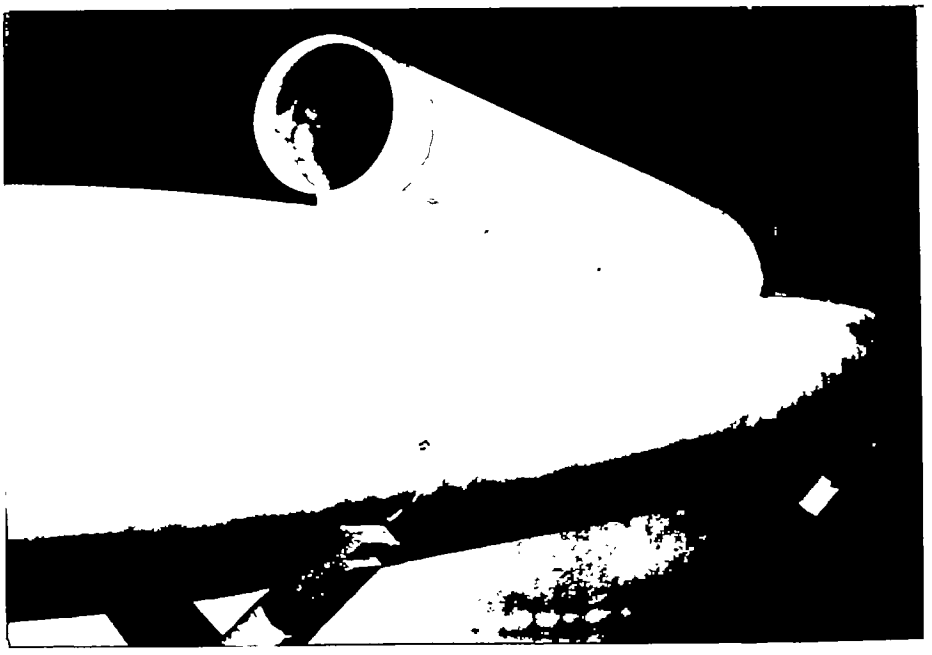

Circular scoop inlet L-83047.1

Semicircular scoop inlet L-83500.1

(b) Close up of scoop inlet, 3/4 front.

Figure 3.- Continued.

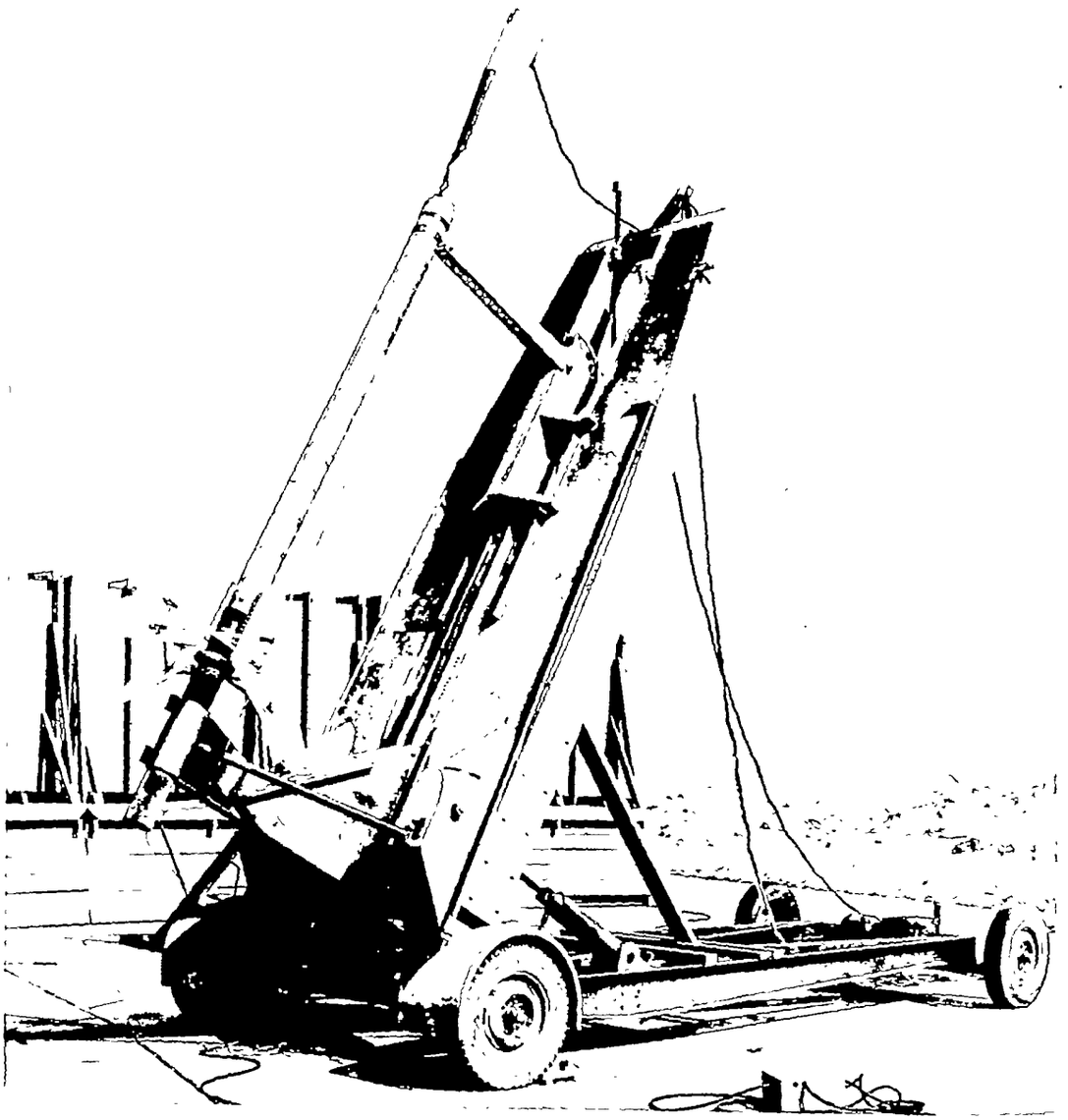

(c) Typical model-booster arrangement. L-84159.1

Figure 3.- Concluded.

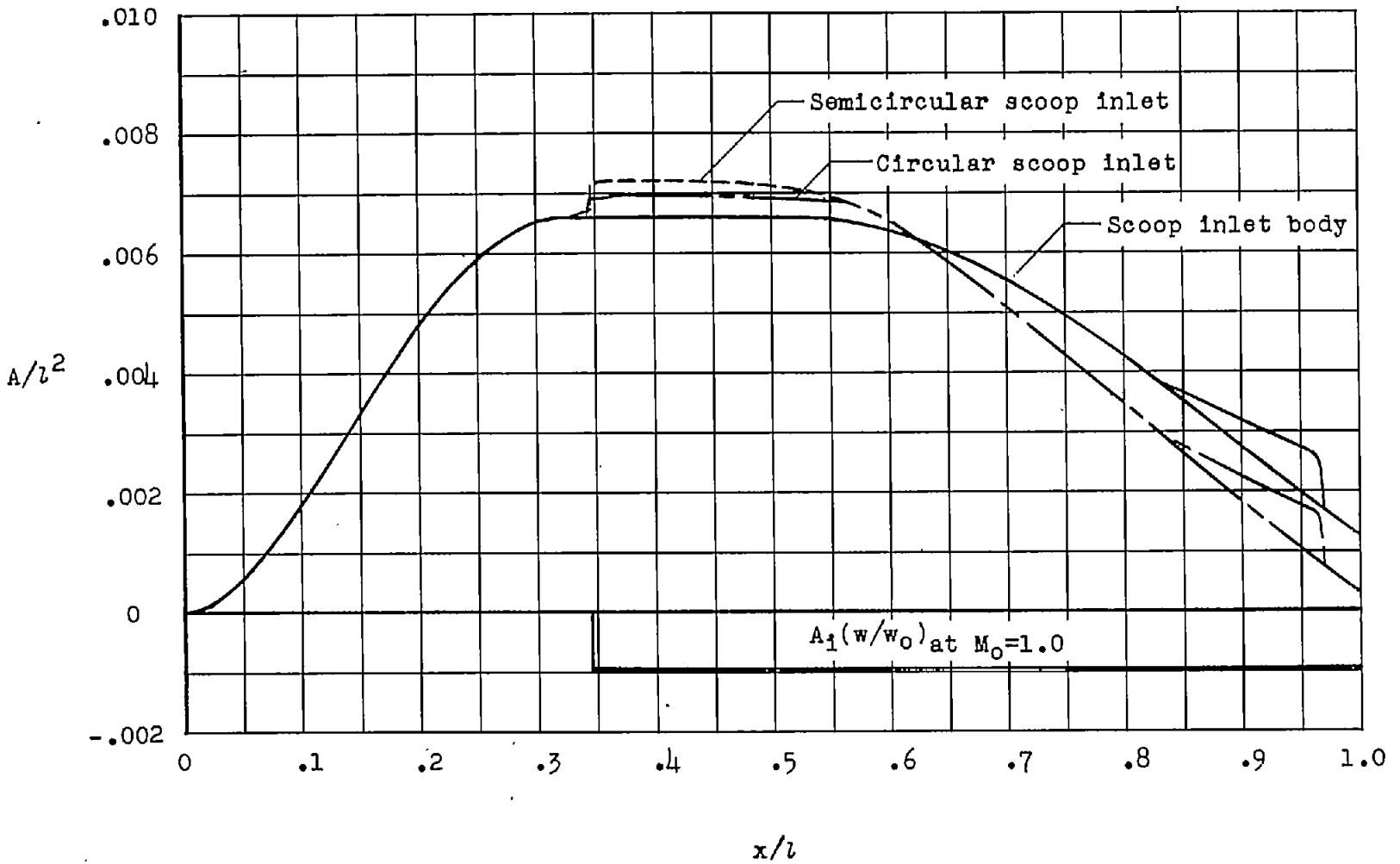

(a) Cross-sectional area distribution.

Figure 4.- Area distribution.

[redacted]

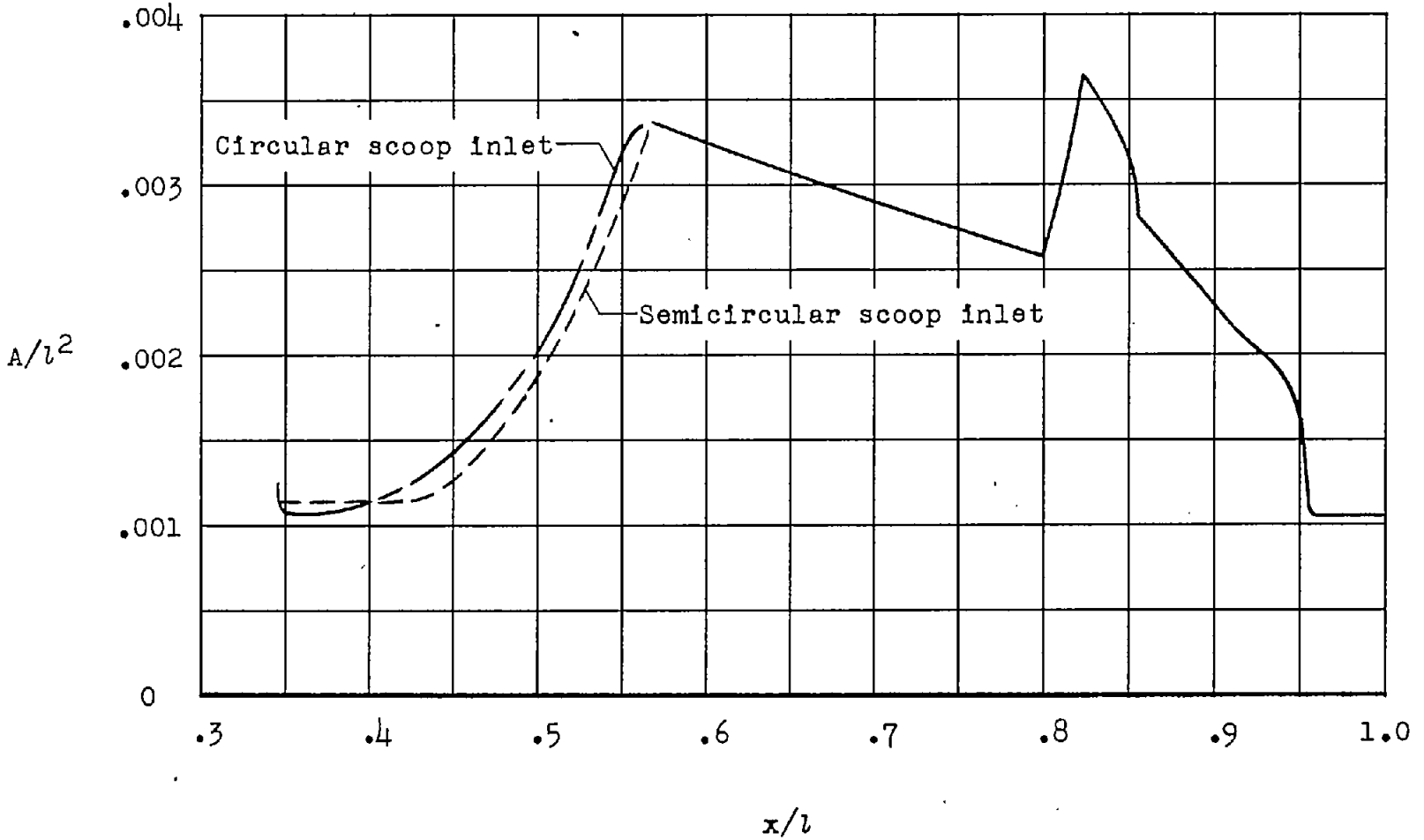

(b) Area distribution of the duct perpendicular to the duct center line.

Figure 4.- Concluded.

[redacted]

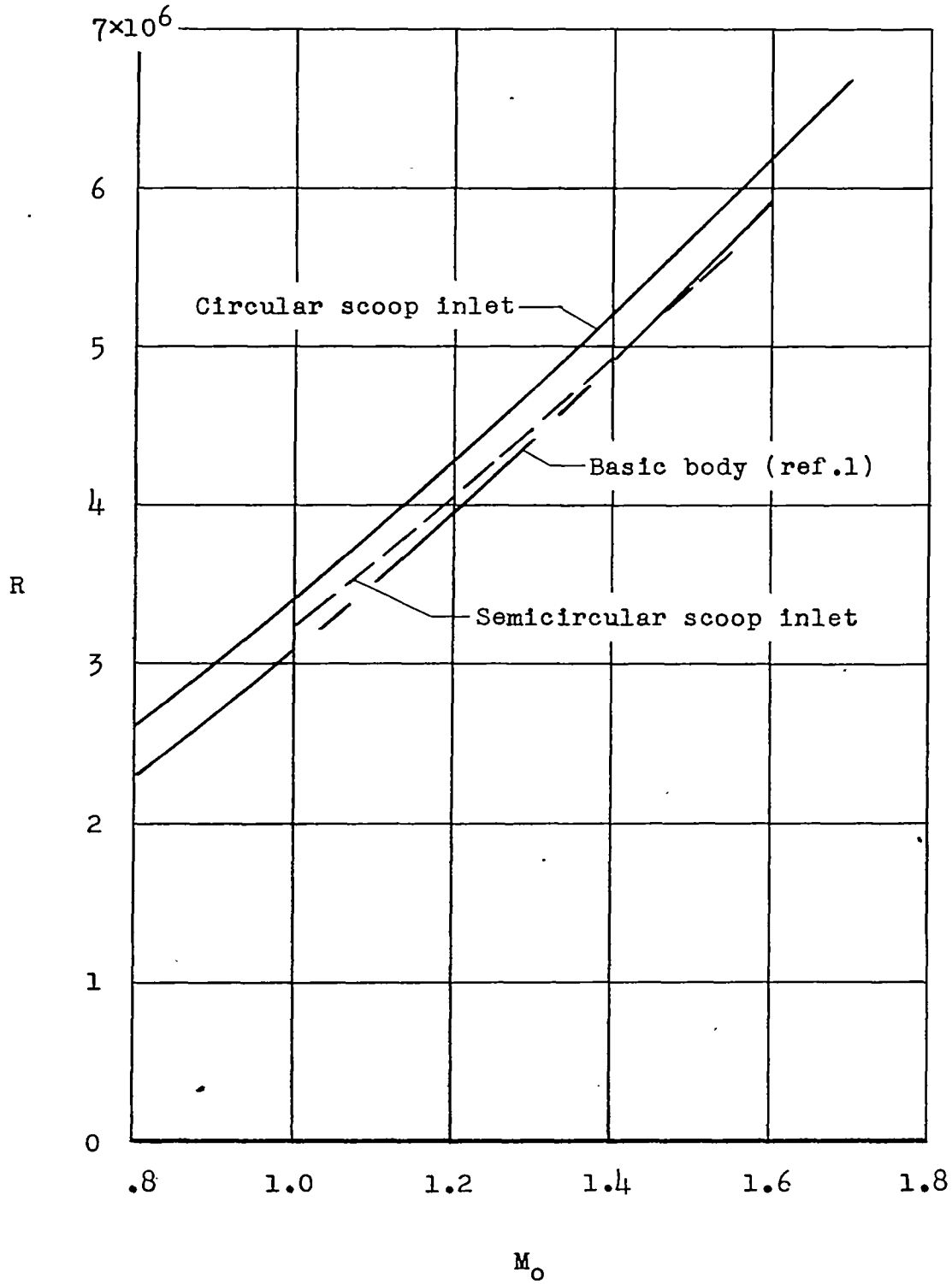

Figure 5.- Variation of Reynolds number, based on body maximum diameter, with Mach number for the scoop-inlet models.

[redacted]

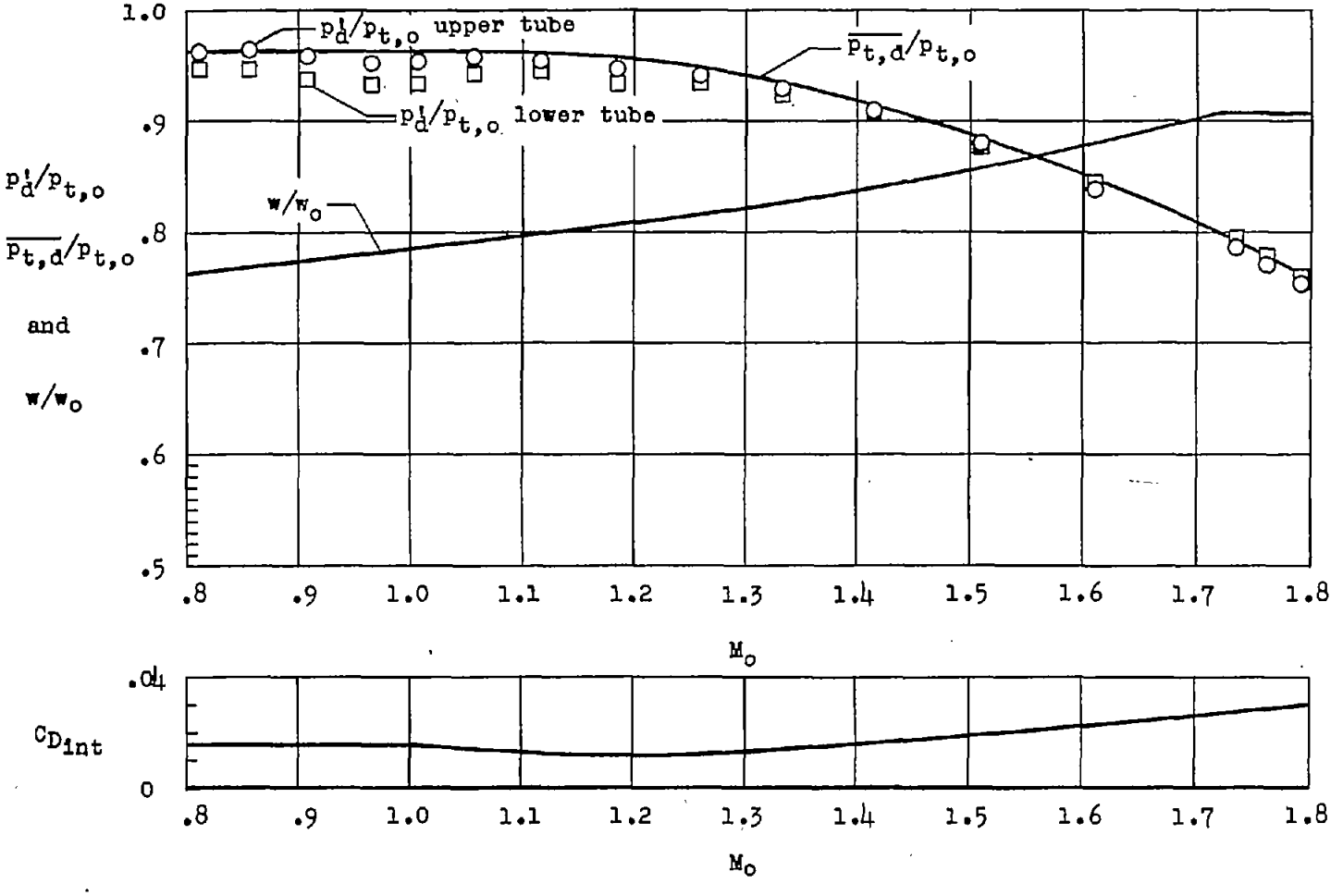

(a) Circular scoop inlet.

Figure 6.- Variation of the total-pressure recovery, mass-flow ratio, and internal drag coefficient with Mach number for the scoop-inlet models.

[redacted]

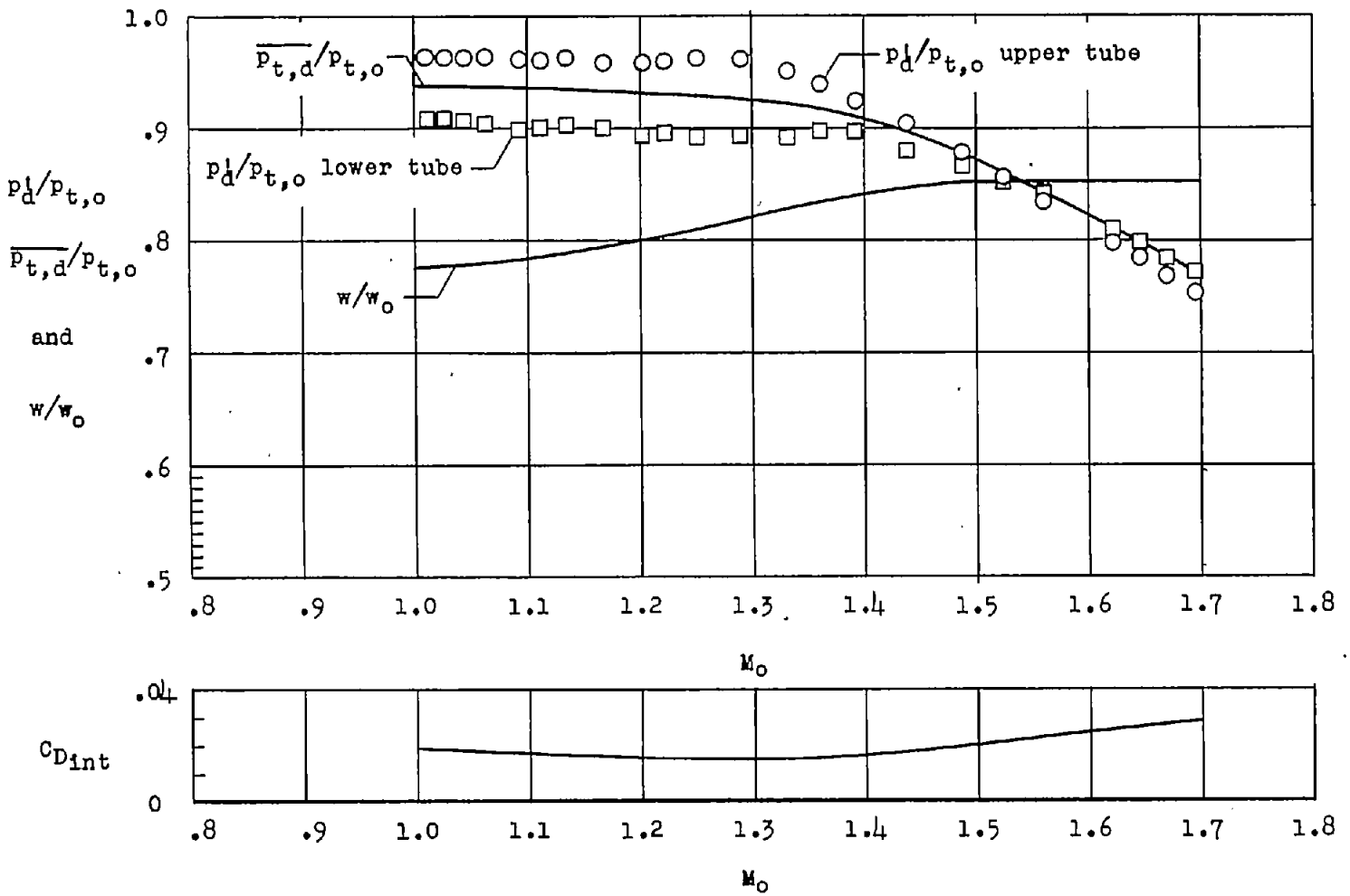

(b) Semicircular scoop inlet.

Figure 6.- Concluded.

[redacted]

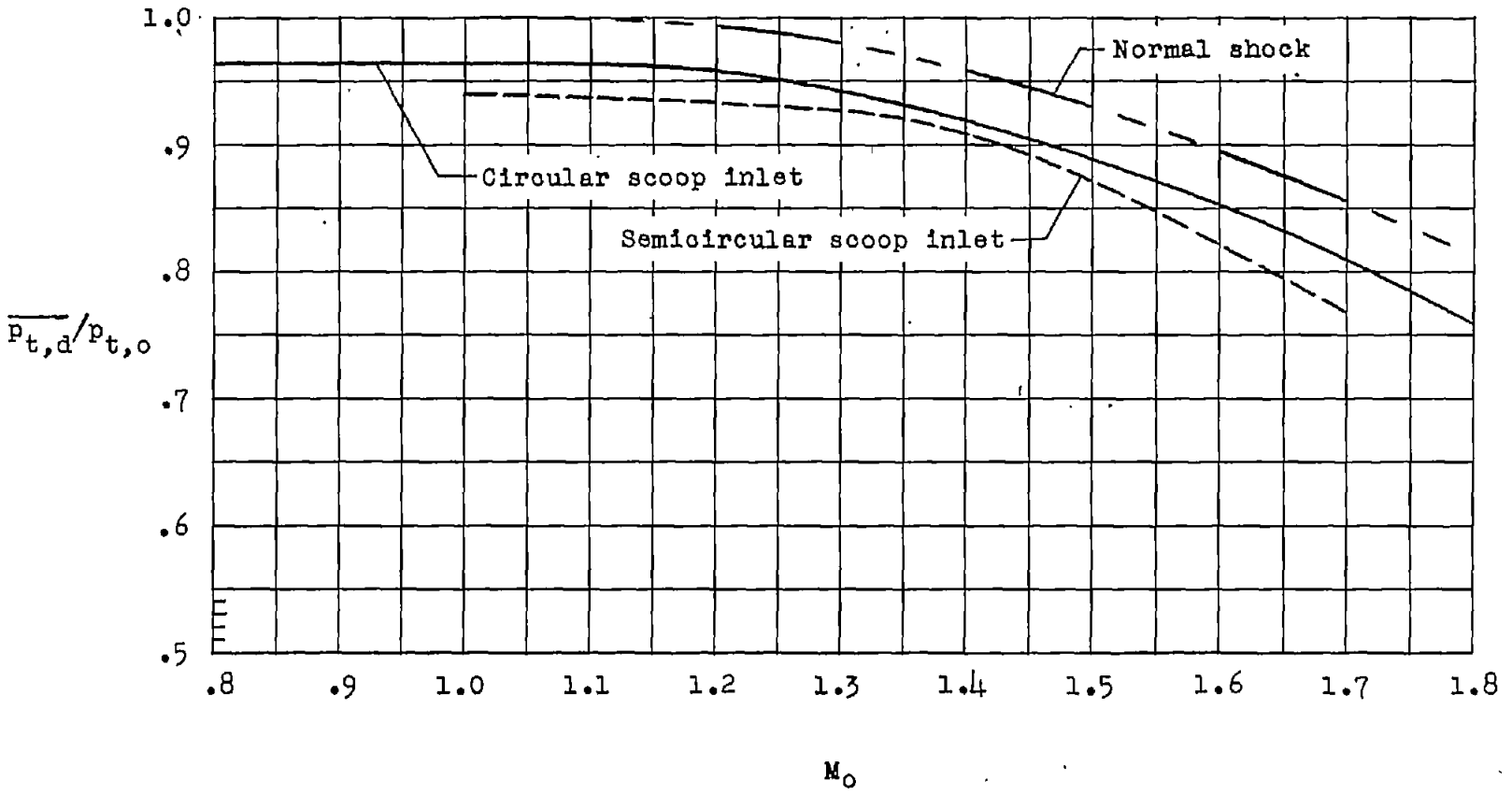

Figure 7.- Variations of the mean total-pressure recovery with Mach number for the scoop-inlet models compared with the normal-shock total-pressure recovery.

[redacted]

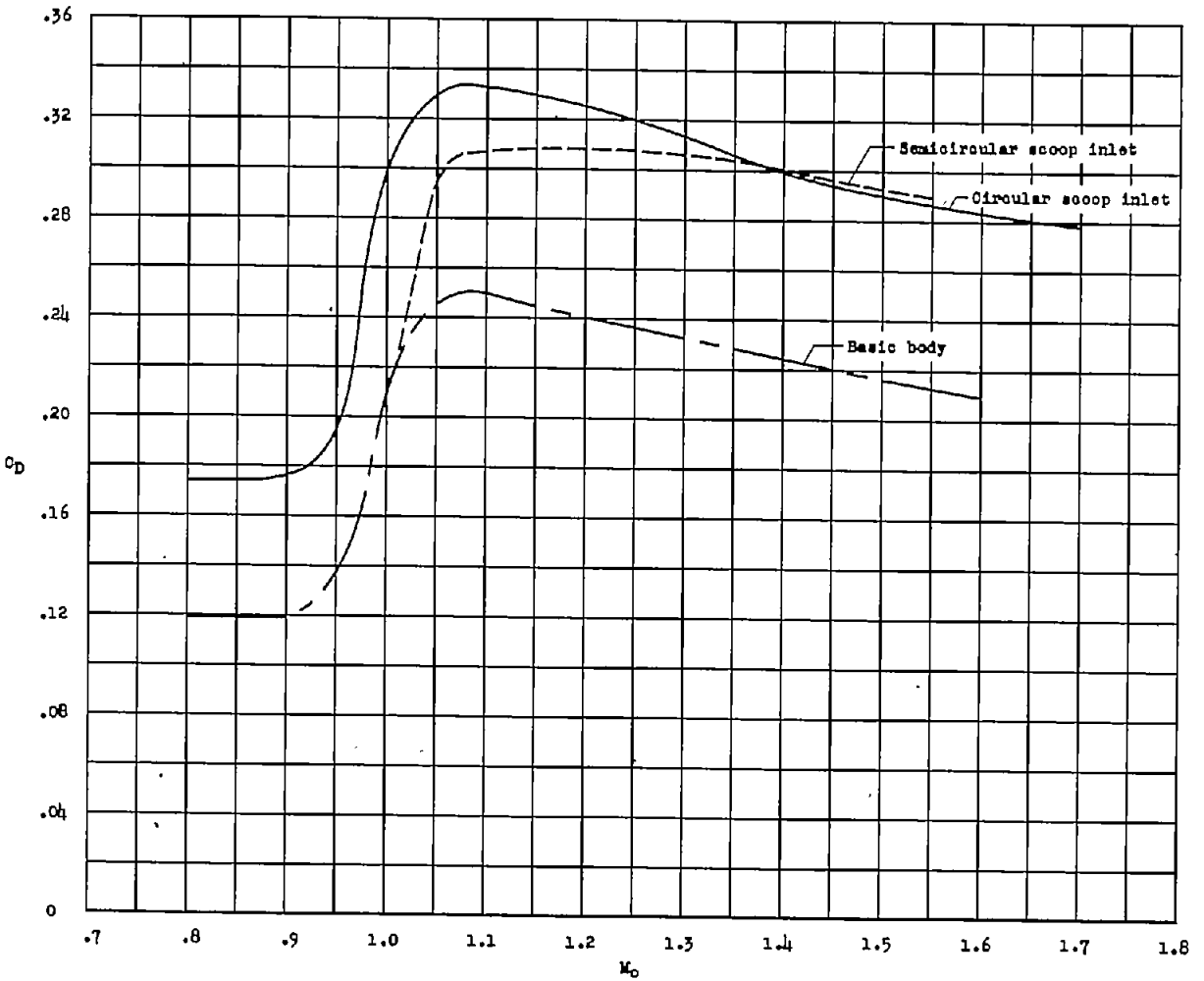

Figure 8.- Variations of the external drag coefficient of the scoop-inlet models and the drag coefficient of the basic body with Mach number.